Project #14074 Defining asperities on faults from spatial variations in fault gouge thickness: Implications for fault strength and rupture mechanics

Jamie Kirkpatrick, *Department of Earth & Planetary Sciences, McGill University, Montréal, Canada*
Kate Shervais, *Department of Geology, State University of New York, Potsdam, NY.*

This project aimed to measure the geometry of the Boyd fault, southern California, to establish the dimension of contact asperities and how the fault roughness evolves with displacement. We mapped the internal structure of the fault using the structure-from-motion methodology. Photographs were taken of extensive cross-sectional exposures of the fault and integrated into a 3-D model using Agisoft's PhotoscanPro. The resulting models were rotated to view the fault down the slip direction and high-resolution images were exported and used to map the edges of the fault core and the principal slip zone, and the boundaries between abandoned principal slip zones within the gouge-filled fault core. Spectral analysis of these contacts showed that the fault slip surfaces smoothed as the fault evolved. However, the smoothing trend is non-linear and scale dependent due to competition between smoothing and reroughening processes. Clasts present within the fault gouge provide a record of the asperities sheared off during deformation. Scale dependent reroughening arises as clasts are sheared off, the fault surface roughens at a scale smaller than the clast dimension, but smoothes at a scale larger than the clast dimension. The maps of the fault core also define the scale of asperities across the slip zone. Geostatistical analysis shows a characteristic length scale of around 3 m where the thickness of the principal slip zone diminishes to sub-millimeter. Together, these results suggest a change in the physical process controlling fault slip occurs after displacements of the order of a few meters.

Technical Report

i. Data collection

The Boyd Fault crops out in Coyote Canyon in the Eastern Peninsular Ranges of southern California, on the west flank of the Coachella Valley (Rowe *et al.*, 2012; previously described as the Coyote Creek fault by Wenk *et al.*, 2000 and the La Quinta Fault by Matti *et al.*, 2006). The fault strike is approximately 300° and it dips ~20° to the northeast. Dip-slip slickenlines on exposed surfaces have an average rake of ~80° from the east. The fault has been mapped over a mapped trace length of ~10 kilometers, and juxtaposes Asbestos Mountain tonalite in the hanging wall and Palm Canyon Metamorphic Complex in the footwall (Sharp, 1979). Pseudotachylyte $^{40}Ar/^{39}Ar$ ages in the hanging wall and footwall of the Boyd Fault indicate brittle faulting during the Laramide at ~56-62 Ma, as well as potential periods around ~70 Ma and 39 Ma (Wenk *et al.*, 2000). Orientations of the pseudotachylytes suggest they formed during reverse slip events (Wenk *et al.*, 2000). Our observations show that the Laramide pseudotachylytes are consistently offset by normal-sense shear fractures and subsidiary faults, but the absolute age of the normal shear fractures is unknown. By analogy with multiple parallel faults dipping shallowly towards the east-northeast, including the West Salton Detachment Fault ~25 km to the south, which have been interpreted as Laramide-era

thrusts reactivated as extensional detachment structures in the Miocene, the Boyd fault may also be a reactivated normal fault (Axen and Fletcher, 1998; Rowe *et al.*, 2012).

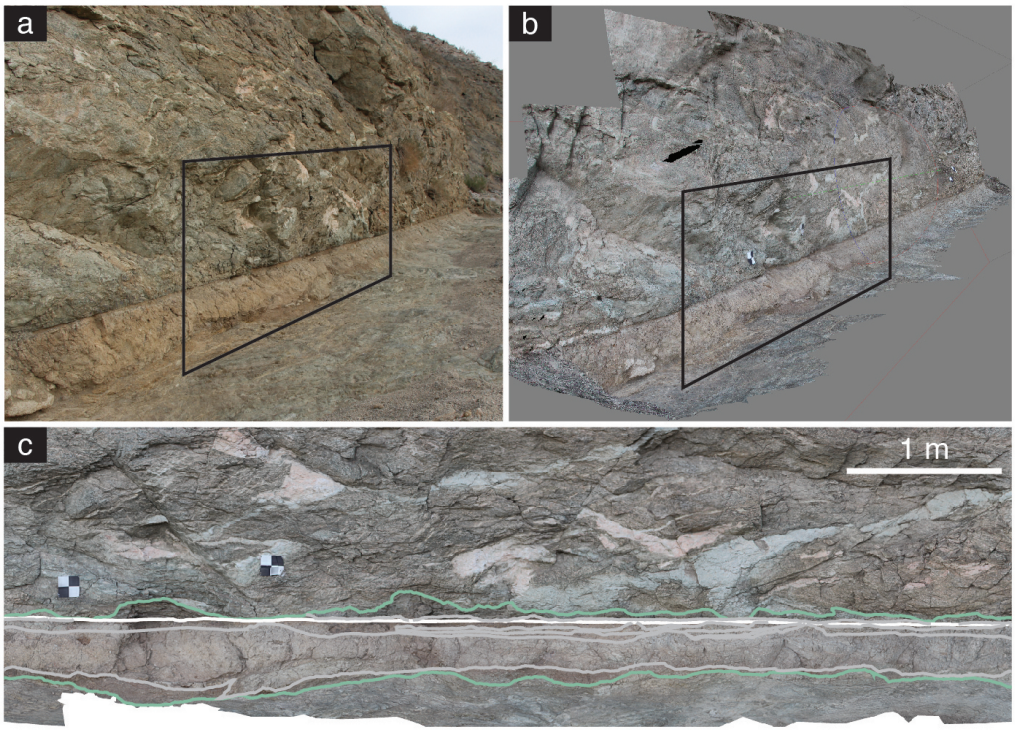

Figure 1. Example of the field workflow used in this study: a.) Photograph of an exposure of the Boyd fault, CA. Around 150 photos similar to this were used to construct the outcrop model. b.) Model generated with Agisoft's PhotoscanPro shown from the same perspective as a. Boxes in a and b show the extent of c. c.) Rectified image exported from PhotoscanPro after the model was rotated to view the exposure down the slip vector. Lines show traces mapped in the field that were used to calculate roughness. White lines are the edges of the principal slip zone and green lines define the extent of the fault core.

We mapped five extensive exposures of the fault located at the base of cliffs in the riverbed of Coyote Canyon, which trends ~305°, approximately the strike direction of the fault. The exposures extend 167 m along strike and provide a high percentage of exposed fault (56.5%) relative to covered areas (43.5%). The internal structure of the fault was mapped using high-resolution rectified images produced with the Structure from Motion (SfM) methodology (Figure 1). SfM uses traditional stereophotogrammetry techniques to build a 3D model with integrated color information of objects or scenes from photographs with large variations in location and view direction (Johnson *et al.*, 2014). Large debris, dust, small pebbles, and organic material were removed from the exposure with a fine brush. The exposures were then extensively photographed, with an average of 5 photographs per meter, and input into Agisoft's PhotoscanPro software (Figure 1a, b). The program generated a 3D model with overlain texture (color) maps of each exposure by matching pairs of points in the images (Verhoeven, 2011; Johnson *et al.*, 2014). High resolution (1.2 mm/pixel) orthorectified images of each exposure were

created by rotating the models to view the exposures in the direction down the slip vector defined by slickenlines on exposed edges of the inner fault core and internal layers (Figure 1c). The true thickness and geometry of the layers is apparent in the resulting cross sections through the fault. The internal structure of the fault was mapped on an iPad in the field at each exposure. These maps were used to measure the geometry and interpret the deformation history of the Boyd Fault.

ii. Analysis

Power spectral density (Brown and Scholz, 1985; Power *et al*., 1988) and variogram analysis were used to quantitatively describe the geometry of the traces of the edges of the principal slip zone and adjacent adjacent abandoned slip zones. These edges are equivalent to surfaces scanned previously with terrestrial laser scanners (e.g. Sagy *et al*., 2007). Our results show that the power spectral density of the edges of these layers is comparable to the previous work, suggesting the SfM methodology applied here is robust. The relative roughness of each contact was evaluated by comparing the power over the range of wavelengths analyzed. The most recent principal slip zone, which crosscuts all other structures in the fault core, is the smoothest. We used crosscutting relations between the abandoned slip zone layers inside the fault core to develop a relative order of formation of the layers. Partitioning the data into segments of layers that formed at the same stage of deformation, we find that the layers do not become progressively smoother; in some cases younger layers are rougher. Furthermore, the relative roughness is scale dependent as some younger layers are rougher at short wavelengths but smoother at long wavelengths.

We interpret these results to be the consequence of scale dependent smoothing and reroughening. Clasts within the gouge of the fault core are the result of asperities on the fault surfaces being sheared off during displacement. Clasts that were sheared off the edges of the fault layers cause embayments to form in the fault surface with dimensions corresponding to the clasts. Inside the embayments, the newly formed fracture surfaces are rough. Clast removal therefore roughens the surface at length scales shorter than the clast dimension. Where clast removal occurs repeatedly, the overall effect is to smooth the surface, as noted previously (e.g. Archard, 1953). Wear of the fault surfaces is therefore scale dependent. Clast long axes range from micrometers to tens of centimeters. The absence of clasts of greater length suggests a change in the physical mechanism of wear at around 1 m dimension.

The experimental semi-variogram (referred to here as the variogram) is a statistical function used to assess spatial continuity of data. The variogram, $\gamma(h)$ is one-half the experimental variogram, 2γ (h) calculated as:

$$\gamma(h) = \frac{1}{2N(h)} \sum_{i=1}^{N} [z(u+h) - z(u)]^2$$

where *z(u)* represents the value of some variable (such as layer thickness) at location *u*, and *z(u+h)* is the value of the same variable at location *u+h*, where *h* is the separation distance (m). *N(h)* is the number of data pairs (e.g. measured layer thickness values) for the particular separation distance, *h*. Therefore $\gamma(h)$ value quantifies the average squared difference between two values separated by *h*. A plot of this function for various separation distances allows for the identification of range and sill values (Kitanidis, 1997).

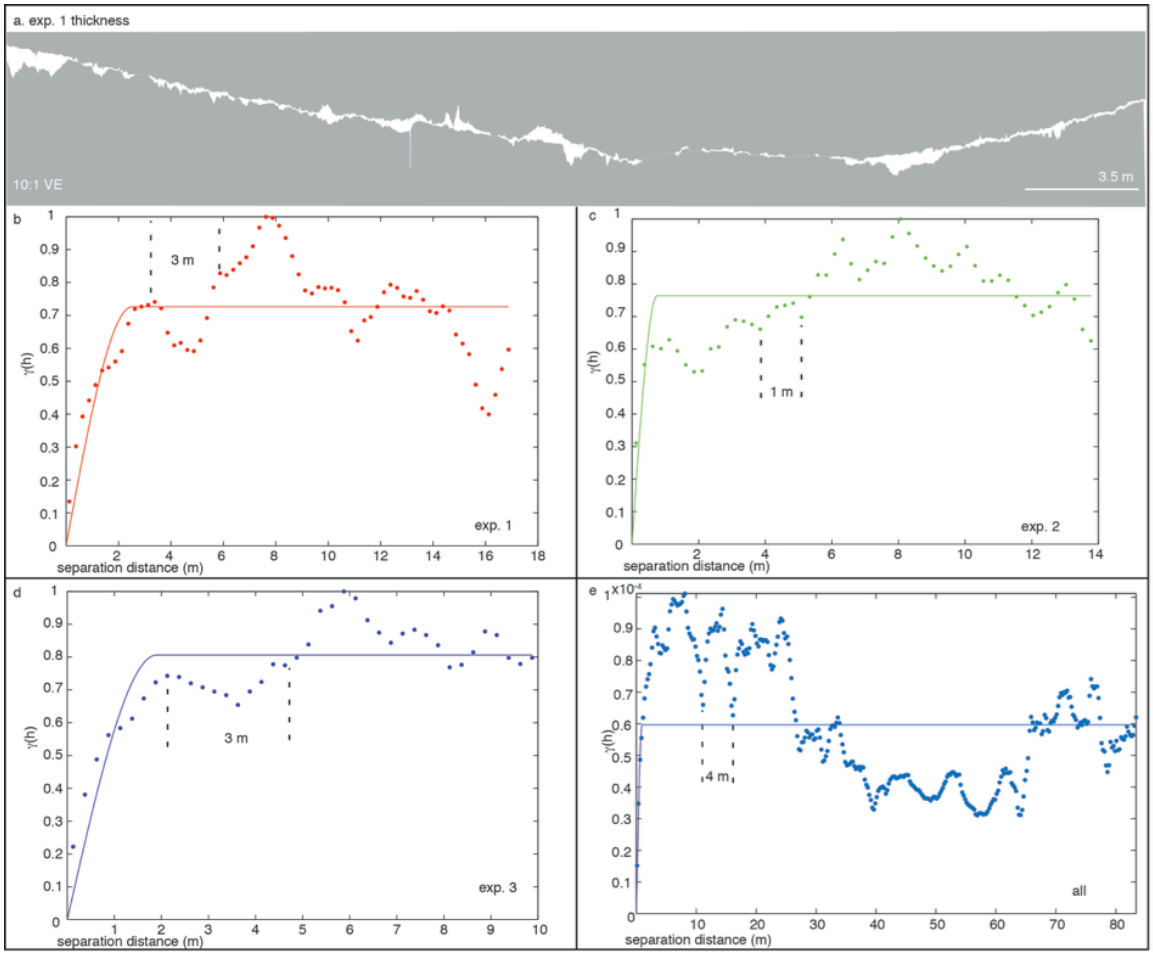

Figure 2. a.) Cross sectional map of the principal slip zone at one exposure with10:1 vertical exaggeration. Note the thickness fluctuations occur approximately every 3 m. b.) c.) d.) normalized slip zone thickness variograms calculated for individual exposures of the principal slip zone. Best-fit spherical models are shown. e.) thickness variogram calculated for the combined dataset (best-fit spherical model is shown). The length scale of periodicity in the thickness fluctuations is shown by the labels in each variogram (1 – 4 m).

The thickness of the principal slip zone fluctuates in a periodic fashion (Figure 2a). Thickness values of this layer show a positively skewed distribution, so we performed a log10-transformation for calculation of the variogram. Variograms of the slip zone thickness from three individual exposures are all fit with spherical models, with ranges of 2.5 m, 0.8 m, and 1.9 m (Figure 2b, c, d). The sills all fluctuate periodically, with wavelengths of 3 m, 1 m, and 2 m. The variogram of the complete data set (maximum

length of 83.7 m) requires a combination model, with a range of 0.9 m, an average of the three individual exposures, and a periodically fluctuating sill of ~4 m (Figure 2e). The ranges and length scales of periodicity in the variograms define the distance over which the slip zone thickness becomes de-correlated and by inspection with Figure 1a correspond to the distances between regions of the fault where the thickness is negligible.

iii. Conclusions

Our results document smoothing of a fault slip surface on a single fault for the first time. However, they also show that smoothing is non-linear with displacement, and arises due to processes that cause scale-dependent smoothing and reroughening. Spatial variations in principal slip zone thickness define the length scale of contact asperities across the fault.

iv. Broader impacts

The intellectual merit of this study is that the results provide a new definition of wear processes on fault surfaces and how they may contribute to fault and rupture mechanics. Using spatial variations in fault core thickness, we have found a characteristic length scale in the fault system defining the length scale of asperities for the first time from field observations. The results also show that fault geometry evolves as faults mature. These observations may explain differences in the source parameters between small and large magnitude ruptures. Our results all contribute to SCEC objective d: Structure and evolution of fault zones and systems: relation to earthquake physics. The insights into rupture mechanics and quantification of asperity dimension are relevant to objective c: Evolution of fault resistance during seismic slip: scale appropriate laws for rupture modeling.

The broader impacts of the work include field training and experience for a graduate student at Colorado State University, who has now successfully defended her master's, and an undergraduate student who is now a graduate student at Colorado School of Mines. Their work in developing and testing the structure-from-motion methodology for this application should prove to be transferrable across the geosciences.

References

Archard, J. (1953), Contact and rubbing of flat surfaces. J. Appl. Phys. 24 (8), 981–988.

Axen, G.J. and J.M. Fletcher (1998), Late Miocene-Pleistocene extensional faulting, northern Gulf of California, Mexico and Salton Trough, California, Int. Geol. Rev. 40, 217–244, doi: 10.1080/00206819809465207.

Brown, S.R. and C.H. Scholz (1985), Closure of random elastic surfaces in contact, J. Geophys. Res., 90 (B7), 5531-5545, doi: 10.1029/JB090iB07p05531.

Johnson, K., E. Nissen, S. Saripalli, J.R. Arrowsmith, P. McGarey, K. Scharer, P. Williams, and K. Blisniuk (2014), Rapid mapping of ultrafine fault zone topography with structure from motion, Geosphere, 10(5), doi: 10.1130/GES01017.1.

Kitanidis, P.K., 1997, Introduction to Geostatistics, Cambridge University Press, 272 pp.

Matti, J.C., D.M. Morton, B.F. Cox, G.P. Landis, V.E. Langenheim, W.R. Premo, R. Kistler, and J.R. Budahn (2006), Fault-bounded late Neogene sedimentary deposits in the Santa Rosa Mountains, southern CA: constraints on the evolution of the San Jacinto Fault, Eos, Trans. AGU, 87(52), Fall Meeting Supplement, Abstract.

Power, W.L., T.E. Tullis, and J.D. Weeks (1988), Roughness and wear during brittle faulting, J. Geophys. Res., 93(B12), 15268-15,278, doi: 10.1029/JB093iB12p15268.

Rowe, C.R., J.D. Kirkpatrick and E.E. Brodsky (2012), Fault rock injections record paleo-earthquakes, Earth Planet. Sci. Lett., 335-336, 154-166, doi:10.1016/j.epsl.2012.04.015.

Sharp, R.V. (1979), Some characteristics of the Eastern Peninsular Ranges Mylonite Zone, in Proceedings of the Conference on Analysis of Actual Fault Zones in Bedrock, Open File Report 79, 258–267.

Sagy, A., E.E. Brodsky and G.J. Axen (2007), Evolution of fault-surface roughness with slip, Geology, 35, 283-286, doi: 10.1130/G23235A.1.

Verhoeven, G. (2011), Taking computer vision aloft -archaeological three-dimensional reconstructions from aerial photographs with photoscan, Archaeo. Prospect., 18, 67–73, doi: 10.1002/arp.399.

Wenk, H.R., L.R. Johnson, and L. Ratschbacher (2000), Pseudotachylytes in the Eastern Peninsular Ranges of California, Tectonophys., 321, 253–277, doi: 10.1016/S0040-1951(00)00064-0.

Presentations

Kirkpatrick, J. D., 'What is an asperity? Insights from the rock record', Seismolab seminar, CalTech, March 2015.

Shervais, K.* and Kirkpatrick, J. D., 'Fault core and slip zone geometry, wear and evolution' AGU Fall Meeting, December 2014, (T14A-03).

Shervais, K.* and J. D. Kirkpatrick, 'Fault core and slip zone geometry, wear and evolution', Southern California Earthquake Center Annual Meeting, Palm Springs, CA, September 2014.

Kirkpatrick, J. D. and Shervais, K.*, 'Fault Surface Geometry, Wear Processes and Evolution: Implications for Earthquake Mechanics and Fault Rock Rheology', Kirkpatrick, J. D. and Shervais, K., Geological Society of America Structural Geology and Tectonics Forum, Golden, CO, June 2014 (*invited*).

Publications

No publications have resulted from this work at this time.